JOURNAL OF SYNCHROTRON RADIATION

Volume 26 (2019)

Supporting information for article:

Implications of disturbed photon-counting statistics of Eiger detectors for X-ray speckle visibility experiments

Johannes Möller, Mario Reiser, Jörg Hallmann, Ulrike Boesenberg, Alexey Zozulya, Hendrik Rahmann, Anna-Lena Becker, Fabian Westermeier, Thomas Zinn, Federico Zontone, Christian Gutt and Anders Madsen

SI - Implications of disturbed photon counting statistics of Eiger detectors on X-ray speckle visibility experiments

Johannes Möller,[a]* Mario Reiser,[a,b] Jörg Hallmann,[a]
Ulrike Boesenberg,[a] Alexey Zozulya,[a] Hendrik Rahmann,[b]
Anna-Lena Becker,[b] Fabian Westermeier,[c] Thomas Zinn,[d]
Federico Zontone,[d] Christian Gutt[b] and Anders Madsen[a]

[a]*European X-ray Free Electron Laser Facility, Holzkoppel 4, Schenefeld Germany,* [b]*University Siegen, Siegen Germany,* [c]*Deutsches Elektronen Synchrotron DESY, Hamburg Germany, and* [d]*European Synchrotron Radiation Facility ESRF, Grenoble France. E-mail: johannes.moeller@xfel.eu*

1. Photon probabilities from both detectors

The artificial increase of double photon events was found for both investigated Eiger detectors. In the main manuscript, the distribution of $P(k)$ as a function of $\langle k \rangle$ was shown for $k = 0, 1,$ and 2 photon events in fig. 3. Additionally, the difference between the expected and measured probabilities was shown in fig. 8. Both figures show data obtained with the commercial Dectris Eiger 4M detector, measured at beamline P10, DESY. The corresponding plot, obtained with the PSI Eiger 500k detector, measured at beamline ID02, ESRF, is shown in fig. 1. As can be seen, the same miscounting effect can be obtained with the second Eiger detector as well. Additionally, this detector can be changed in bit counter depth and therefore frame rate. There was no influence found of counter depth on the reported miscounting effect.

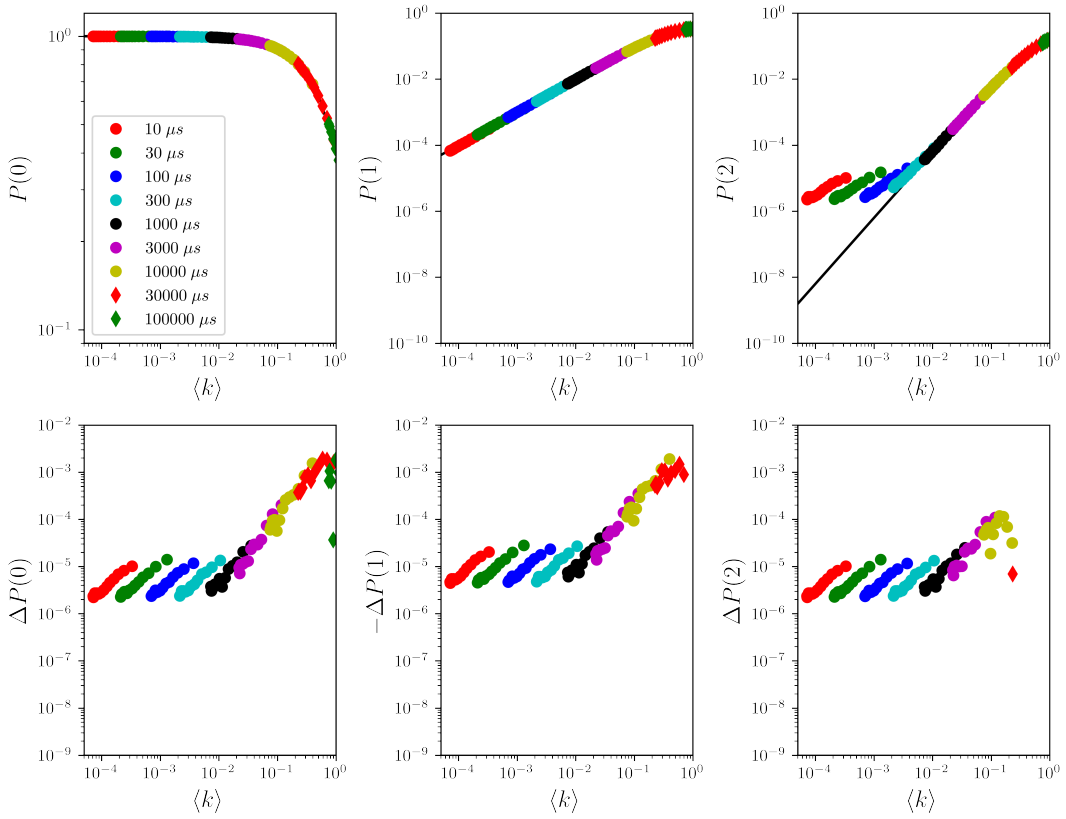

Fig. 1. Top row: Distribution of photon count probabilities as a function of number of photons per pixel $\langle k \rangle$, measured with the PSI Eiger 500k at beamline ID02, ESRF. In black, the expected Poisson-Gamma distribution is plotted. Bottom row: Difference between expected and measured photon count probabilities for $k = 0, 1$ and 2 photons.

2. Correction schemes

From eq. 16 in the main manuscript as well as the CASE I and II described in section 4.2, three different equations can be calculated which apply the correction parameter κ to obtain the corrected contrast β_0. These are displayed in the following.

From eq. 16, one obtains directly:

$$\beta_0 = \frac{P(0)}{P(1)} - \frac{1 + 2 * \kappa(t)}{\langle k \rangle} \tag{1}$$

CASE I:

$$\beta_0 = \frac{P(0)}{P(1) + \kappa(t)\,\langle k\rangle} - \frac{1}{\langle k\rangle - \kappa(t)\,\langle k\rangle} \tag{2}$$

CASE II:

$$\beta_0 = \frac{P(0) - \kappa(t)\,\langle k\rangle}{P(1) + 2\kappa(t)\,\langle k\rangle} - \frac{1}{\langle k\rangle} \tag{3}$$

The three equations correspond to the three plots displayed in fig. 7 in the main manuscript.

3. Detector linearity

We additionally validate the two cases against the overall intensity measured on the detector. As case I adds photons whereas case II preserves the absolute photon number, these should also be distinguishable in $\langle k\rangle$. Fig. 2 a) displays the mean number of photon per pixel, normalized on the exposure time, absorber transmission and incoming intensity of the beamline. As can be seen, a clear dependence of the attenuator setting can be seen, whereas there is only a small dependence on the exposure time visible. We can not exclude that the different attenuators have slightly different thicknesses, which would result in different transmissions. Therefore, we normalized the measured intensities for each attenuator setting on the mean intensity measured for exposure times 1 ms $\leq t \leq$ 10 ms. This is displayed in fig. 2 b).

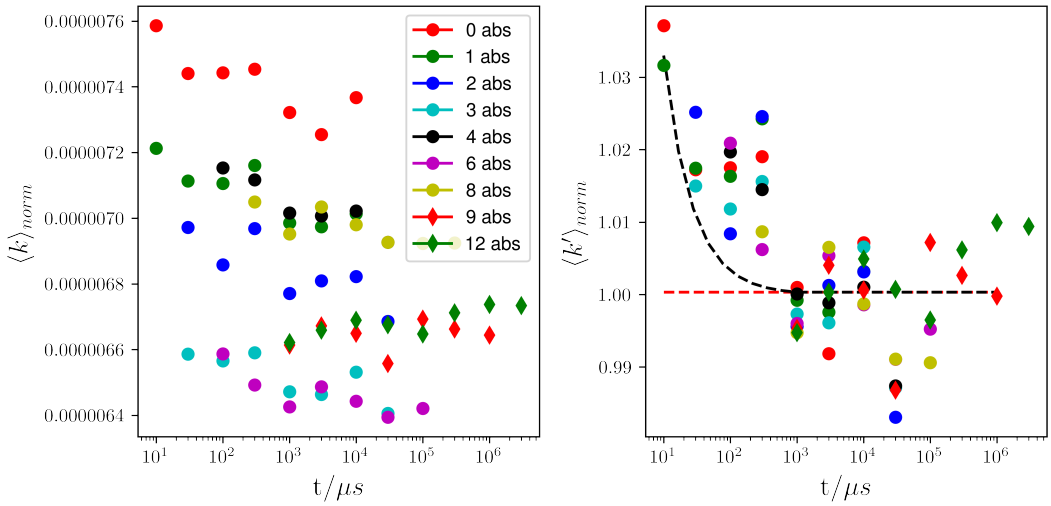

Fig. 2. a) Mean number of photons registered per pixel, normalized on the incoming flux, exposure time and absorber transmission. b) Data also normalized on $\langle k_{norm} \rangle$ for exposure times of $t = 1$ ms $\leq t \leq 10$ ms.

An increasing intensity towards smaller exposure times can be observed, favoring in this case scheme I in order to explain the origin of the additional double photon events. The expected dependencies of $\langle k \rangle$ on the exposure time are additionally plotted for both cases. Case I is shown in black, case II in red.

In contrast to both cases, the data shows a step like intensity increase towards shorter exposure times below 1 ms, with an additional increase for $t < 100$ μs. Even though case I involves an increase in $\langle k \rangle$, neither of the two cases explains the step like increase in intensity for exposure times $t < 1$ ms. Additionally, such a step like dependence on the exposure time has not been observed for any of the previously shown quantities. Therefore, it remains unclear if this increase in intensity is related to the artificial increase of the contrast.

4. Threshold and read out mode

We additionally investigated the dependence of the miscounting on the selected read out mode and threshold level. The value of κ was calculated from the photon count statistics following eq. 18. The measurements were done with the Eiger 500k module at beamline ID10, with an X-ray energy of 8 keV. In general, the threshold values is set to at least half of the X-ray energy. We additionally increased the threshold value from 4 up to 6 keV. As can be seen, the probability of miscounting κ decreases with increasing threshold value. However, this might be explained by the lower number of double counts which are detected the higher the threshold is set. Still, the reported miscounting can not be suppressed by changing the threshold value or read out mode.

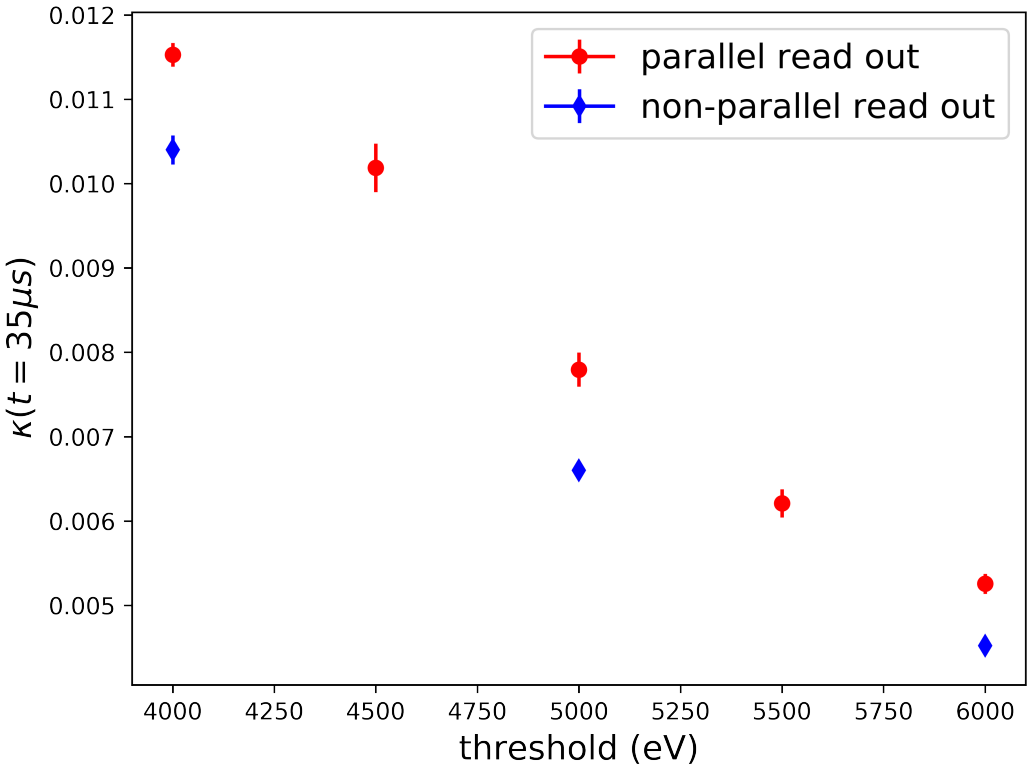

Fig. 3. Dependence of the correction parameter κ on the set threshold value and read out mode.

5. XSVS on silica particles

In the main manuscript, the XPCS and XSVS results on silica particle are shown on a logarithmic scale, in order to illustrate the difference between corrected (black) and uncorrected (green) contrast values. The corresponding plot on a linear scale is shown in fig. 4.

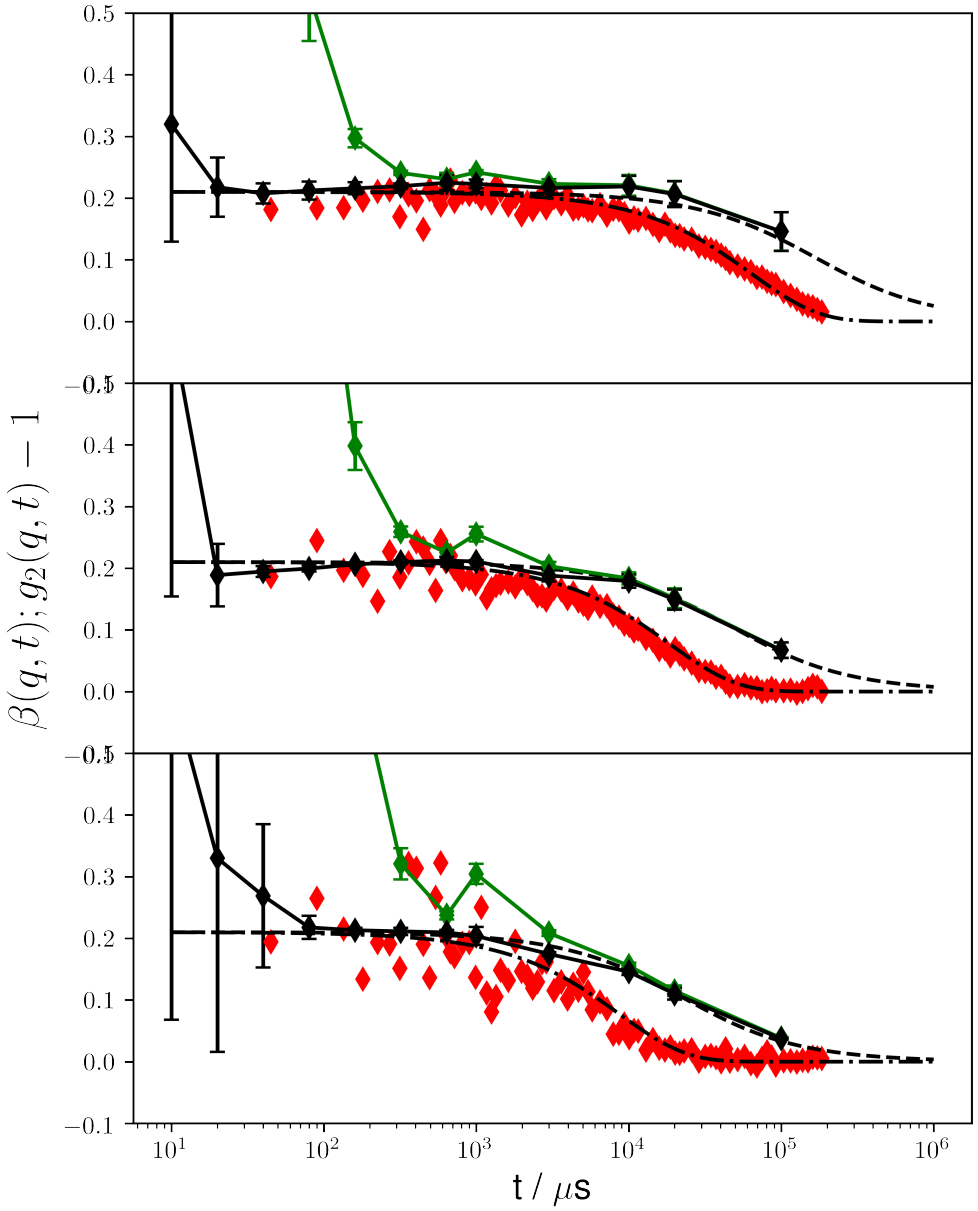

Fig. 4. XPCS and XSVS measurements on 100 nm silica particles at q-values of 1.75 10^{-2} nm^{-1}, 3.25 10^{-2} nm^{-1}, and 4.75 10^{-2} nm^{-1}. The green data points correspond to the uncorrected and the black data points to the corrected XSVS results.